CO_2 gasification of sugarcane bagasse char: consideration of pyrolysis temperature, silicon and aluminum contents, and potassium addition for recirculation of char

Ingrid Lopes Motta[a,†], *Ross A. Arnold*[a,††], *Francisco Javier Lopez-Tenllado*[a], *Rubens Maciel Filho*[b], *Maria Regina Wolf Maciel*[b], *Josephine Mary Hill*[a,*]

[a]Department of Chemical and Petroleum Engineering, Schulich School of Engineering, University of Calgary, 2500 University Drive, Calgary, AB T2N 1N4, Canada

[b]Laboratory of Optimization, Design, and Advanced Control, School of Chemical Engineering, University of Campinas, Av. Albert Einstein 500, Campinas, 13083-852, Brazil

KEYWORDS

sugarcane bagasse; gasification; char; TGA; ball milling; catalyst; potassium

ABSTRACT

In sugarcane bagasse gasification, char recirculation to the gasifier improves syngas quality and process efficiency. To determine the effect of char properties on reaction kinetics, in this work the pre-gasification pyrolysis temperature, particle size, and catalyst (potassium) loading were varied. Char samples were prepared at 750-900 °C via pyrolysis and gasified isothermally in a thermogravimetric analysis unit at 850 °C with CO_2, and gasification data was modeled using the random pore and extended random pore models. Increasing pyrolysis temperatures did not affect char morphology and surface composition but did reduce the surface area as determined by N_2 adsorption, decreasing initial gasification rates and the overall fitted rate constants. Reduction of the particle size via ball milling decreased the time required for complete conversion and changed the shape of the rate versus conversion curves from monotonically decreasing to concave down. The char sample prepared via pyrolysis at 900 °C was an exception, having a maximum rate at ~10% conversion without ball milling. After ball milling of the char sample prepared at 750 °C, there was an accumulation of ash (Al and Si) on the surface of the particles and a reduction in the surface area, consistent with the ash blocking pores – the porosity in these samples increased during the initial stages (up to ~20% conversion) of gasification. The gasification behavior was generally well modeled by the extended random pore model. Although the addition of KOH (K/Al mass ratio ~ 0.2-1.25) enhanced the gasification rates, too much K - from the addition of KOH or after 90% conversion - created mass transfer limitations resulting in lower gasification rates.

1 Introduction

Sugarcane bagasse is the solid residue of the extraction of juice from sugarcane,[1] with approximately 300 kg of sugarcane bagasse produced for every tonne of sugarcane processed.[2] Despite the low cost and high availability, sugarcane bagasse is usually underused in low-added-value applications such as heat and power production in cogeneration plants.[3] An alternative use for sugarcane bagasse is as a feedstock for gasification processes. Although the majority of the carbon feed will be converted to gaseous and liquid products (85-95 wt% from 720-840 °C in industrial circulating fluidized bed gasifiers),[4] some solid residue will remain. This residue, referred to as char (or biochar since it was obtained from biomass), can be used in various applications, such as soil remediation, carbon sequestration, and wastewater treatment,[5,6] but also can be recirculated in the gasifier to improve the cold gas efficiency of the reactor and increase the syngas heating value.[7] The char properties depend on the gasifier conditions (e.g., temperature and catalyst), and may affect gasification rates during recirculation.

Previous gasification studies of sugarcane bagasse char[8–12] were performed under non-isothermal conditions that are dissimilar to the conditions within circulating fluidized bed gasifiers. Nonetheless, authors of these studies suggested that temperatures above 800 °C removed hydroxyl, aliphatic C-H, and olefinic C=C groups, and that increasing pyrolysis temperatures affected the char physical structure such that the reactivity was reduced.[9,10] Char reactivity generally increases with surface area (i.e., increased contact between gasifying agents and carbon sites)[13] and, for the biochar materials studied thus far (e.g., oak, pine, grass;[14] soybean stover, peanut shell;[15] pig manure, wheat straw;[16] Douglas fir, hazelnut shell[17]), maximum surface areas were achieved up to a pyrolysis temperature of ~700 °C.[14–17] Specific surface areas on a per mass basis are also a function of particle size. Within the laboratory,

particles can be ball milled to reduce their size, and previous studies in which sugarcane bagasse char was ball milled focused on adsorption applications,[18–20] precursors for carbon electrodes,[21] and polymer composites.[22] The milling reduced the particle size of sugarcane bagasse char from above 100 μm to 100-500 nm,[18,19,22] increased the char surface area from 51 to 331 m^2/g for char samples prepared at 450 °C,[19,20] and added oxygen functional groups to the surface by creating open ends of the carbon chains which are exposed to the atmosphere,[19,20] which may improve the char gasification performance.

Alkali metals such as potassium participate in the oxygen transfer cycle and catalyze gasification.[23] Potassium is mobile within and between particles but this mobility can be hindered by the presence of elements other than carbon. For example, Si and Al deactivate K through the formation of aluminosilicate species (e.g., $KAlSiO_4$).[24] Al is typically present in lower amounts than Si in gasification feeds, and thus Al is the limiting reactant in potassium aluminosilicate formation. Feedstocks usually require K/Al ratios higher than 0.5[25,26] or the addition of alkaline earth species such as Ca that preferentially react with Si and Al[25] to ensure that there is sufficient K to catalyze the gasification. Sugarcane bagasse contains 1.3 wt% SiO_2, 0.2 wt% Al_2O_3, and 0.4 wt% CaO (calculated based on sugarcane bagasse ash content and ash elemental composition determination)[1] and so the appropriate catalytic amount of potassium has to be determined.

The current study was undertaken to determine how pyrolysis above 700 °C, char particle size, Si and Al contents, and K addition affect the gasification rates of sugarcane bagasse char at isothermal conditions. The char samples were prepared via pyrolysis at different temperatures (750, 800, 850, or 900 °C) and gasified at 850 °C with CO_2 in a thermogravimetric analysis unit. Some of the char samples were ball milled before gasification, with or without KOH, aiming to

reduce particle size, increase surface area, and reduce mass transfer limitations. In the char samples with added KOH, ball milling was performed to improve K dispersion. Kinetic modeling and model discrimination techniques were used to quantitatively relate the gasification performance to the physical and chemical properties of the char samples.

2 Experimental Section

2.1 Sugarcane bagasse collection and characterization

Sugarcane bagasse samples were collected at the sugar mill USJ in Araras (São Paulo, Brazil) in April 2019, dried (reducing moisture content from 60 to 6 wt%) and sieved using Tyler test sieves. Proximate analysis was performed via macro thermogravimetric analysis (TGA) as per ASTM D7582 in an automatic multiple sample thermogravimetric analyzer TGA-1000 (Navas Instruments, Conway, USA) with approximately 500 mg of each sample. Ultimate analysis was conducted via CHNOS chemical analyses in a Vario Macro Cube analyzer (Elementar, Hanau, Germany) with ~80 mg of sample that was placed onto a tin sheet, molded into a capsule, and then combusted at 1150 °C. The produced gases (N_2, CO_2, H_2O, and SO_2) were quantified by gas chromatography with a thermal conductivity detector (GC-TCD).

For scanning electron microscopy (SEM) analysis, samples were transferred to double-sided carbon tape fixed to stubs and sputter-coated in a coating system model K450 (EMITECH, Kent, United Kingdom) with gold (20 nm film) under vacuum for 2 min. The samples were analyzed in an SEM model Leo 440i (LEO Electron Microscopy, Cambridge, England) with an energy dispersive X-ray (EDX) detector (Cambridge, England) for measurements at 20 kV and 100 mA (SEM imaging) or 800 mA (EDX analysis). In addition to observing the sample morphology, particle size distributions were calculated from the SEM images by measuring at least 200

106 particles. EDX analysis was used to map at least five different regions to obtain average
107 elemental compositions from which the K/Al and K/C ratios on the char surfaces were
108 calculated. K/Al and K/C ratios were analyzed because K is the most active species for
109 gasification, Al is the limiting reactant in the formation of potassium aluminosilicates, and C is
110 the substrate to undergo gasification. The standard deviations of the compositions are reported
111 (Table 1 and Table 2).
112
113 2.2 Char preparation and characterization
114 Char samples were prepared via pyrolysis in a quartz reactor (ID = 25 mm), placed in a
115 furnace (Mellen, Concord, USA) connected to a scrubber containing methoxy-propanol and
116 water to trap any tar or syngas produced. Approximately 4 g of sugarcane bagasse was heated at
117 25 °C min^{-1} in flowing N_2 (185 mL min^{-1}) to the desired temperature (750, 800, 850, or 900 °C).
118 The pyrolysis temperatures were selected based on the typical temperature ranges of circulating
119 fluidized bed gasifiers. The sample was maintained at the pyrolysis temperature for 2 h before
120 being cooled to room temperature. The char preparation yield, Y, was determined by eq. (1),
121 where m_f and m_0 refer to the final and initial masses, respectively.

$$Y = \frac{m_f}{m_0} \tag{1}$$

122 A portion of each char sample was ball milled in a Pulverisette 6 planetary mono mill (Fritsch,
123 Idar-Oberstein, Germany) for 3 h at 500 rpm with zirconia balls of 5 mm diameter. The rotation
124 direction was altered every 30 min to increase homogenization. The char sample prepared at 750
125 °C was ball milled without KOH (K/Al = 0.2 [molar basis], KOH loading of 0 wt%) and with
126 different amounts of KOH (K/Al = 0.5, 1.0, and 1.25, KOH loadings of 19, 53, and 70 wt%,
127 respectively). The char samples were named according to the pyrolysis temperature (e.g.:

char750 refers to a sample prepared at 750 °C). The char samples after ball milling have the prefix "BM" and, if the sample was ball milled with KOH, its target K/Al ratio is indicated (e.g., BM-char750 with K/Al = 0.5 refers to a sample pyrolyzed at 750 °C and then ball milled with KOH at a target K/Al molar ratio of 0.5).

All char samples were analyzed with N_2 and CO_2 adsorption to determine surface area, micropore volume, and pore size distribution. First, the samples were degassed using a sample degas system VacPrep 061 (Micromeritics, Norcross, USA) under a vacuum of 100 μm Hg (13.3 Pa) at 200 °C for 18 h. The samples were then transferred to the adsorption analyzer Tristar II Plus (Micromeritics, Norcross, USA) for N_2 adsorption analysis at -196 °C, followed by CO_2 adsorption at 0 °C. The surface areas were determined with the SAIEUS software (Micromeritics, Norcross, USA) using the two-dimensional nonlocal density functional theory (2D-NLDFT) fitting with N_2 and CO_2 adsorption data and λ values of 2.0-3.0, as well as with the BET equation using N_2 adsorption results. N_2 and CO_2 adsorption data was also used to obtain pore size distributions via 2D-NLDFT, and CO_2 adsorption data was used to calculate micropore volumes with the Dubinin-Radushkevich equation.

The surface functional groups of four char samples (char as prepared at 750 and 850 °C both prior to and following ball milling) were determined with a Fourier Transform Infrared spectrometer (FTIR, Nicolet iS50, Thermo Scientific, USA) with an attenuated transmission reflectance (ATR) attachment. ATR spectra were collected in the 4000 to 400 cm^{-1} wavenumber range, accumulating 32 scans at a 2 cm^{-1} resolution.

Ash contents were determined as per ASTM D3174 in an SDT Q600 thermogravimetric analyzer (TA Instruments, New Castle, USA). The SEM-EDX analyses of the char samples followed similar protocols to those used for the sugarcane bagasse samples except that a different

151 instrument was used (Phenom ProX instrument, Thermo-Fisher, 15 kV, Eindhoven, Netherlands)
152 and the samples were not sputter-coated before analysis.
153 All samples were stored at ambient conditions between char preparation via pyrolysis and
154 gasification tests. As sample devolatilization is complete by 600 °C[27] and pyrolysis was performed
155 at a minimum temperature of 700 °C, sample storage did not further affect the volatile content of
156 the char.
157
158 2.3 Gasification experiments
159 The gasification experiments were conducted in a benchtop TGA (SDT Q600, TA Instruments,
160 New Castle, USA) with 3.5 mg of sample in an alumina crucible. Each experiment consisted of
161 heating to the gasification temperature (850 °C) under an inert N_2 atmosphere (200 mL min^{-1})
162 with a heating rate of 20 °C min^{-1}. Once the system reached 850 °C, isothermal char gasification
163 proceeded with a CO_2 flow of 200 mL min^{-1} and N_2 flow of 5 mL min^{-1} to prevent backflow of
164 the CO_2 over the TGA balance. The gasification temperature of 850 °C is within the operating
165 range of fluidized and fixed bed gasifiers (750-950 °C). The gasification rates with CO_2 are
166 similar to those with steam, as shown in previous studies on petcoke and sugarcane bagasse co-
167 gasification under CO_2[8] and steam[28] atmospheres.
168 The TGA data for gasification was analyzed and treated as follows: the time, *t*, versus mass, *m*,
169 data was smoothed to 1000 points using the locally estimated scatterplot smoothing (LOESS)
170 technique in SigmaPlot 14.0 with a polynomial order of 3 and weighted according to 5% of the
171 neighboring data. The reduced data was used to calculate several kinetic parameters. The sample
172 and carbon conversions in the gasification stage were calculated using eqs. (2) and (3),
173 respectively, where the subscripts *0*, *t*, and *f* denote the sample mass at time zero, time *t*, and at

the end of the experiment, respectively. The carbon reaction rates were calculated by eq. (4) using numerical integration, where the subscripts *1* and *2* denote two consecutive time points one second apart, while *Ash* denotes the mass fraction of ash in the sample.

$$X_{sample} = \frac{m_{sample,0} - m_{sample,t}}{m_{sample,0} - m_{sample,f}} \tag{2}$$

$$X_{carbon} = \frac{X_{sample}}{1 - Ash} \tag{3}$$

$$\frac{dX_{carbon}}{dt}(t_1) = \frac{X_2 - X_1}{t_2 - t_1} \tag{4}$$

2.4 Kinetic modeling and model discrimination

The gasification data was modeled using the random pore model (RPM, eq. (5))[13] and the extended random pore model (eRPM, eq. (6)).[29]

$$\frac{dX}{dt} = k_j (1 - X)\sqrt{1 - \psi \ln(1 - X)} \tag{5}$$

$$\frac{dX}{dt} = k_j (1 - X)\sqrt{1 - \psi \ln(1 - X)}[1 + c(1 - X)^p] \tag{6}$$

In eqs. (5) and (6), k_j is the rate constant, ψ is the structural factor,[13] and c and p are two semiempirical parameters.[29] During gasification, pores develop within the carbon structure, increasing the surface area. The developed pores collapse as gasification proceeds, reducing the surface area. The structural factor ψ represents the difference between the initial and maximum surface areas during gasification.[13] The parameters c and p relate to the value and position of the maximum gasification rate, respectively, yielding a better fit of the mathematical model.[29] Athena Visual Studio v14.2 was used in the kinetic modeling and model discrimination.

In the kinetic modeling, k_j, ψ, c, and p were determined using the nonlinear least-squares method. The RPM and eRPM were fit to the gasification rates (dX_{carbon}/dt) as a function of carbon conversion (X_{carbon}) by minimization of the residual sum of squares (*RSS*) with an experimental error of 10%. The modeling required data with equally-spaced conversions to avoid the overrepresentation of data points at high conversion levels and allow a better fit.[30] The model discrimination was performed using the Akaike information criterion (*AIC*), defined in eq. (7), where m is the number of estimated parameters, n is the number of observations (1000 for both models), and *RSS* is the residual sum of squares. The models were also compared with the calculation of the Akaike probability share (π_{AIC}), shown in eq. (8), where L_k is the relative likelihood of model k, which is defined by eq. (9).

$$AIC = m\frac{2}{n} + \ln\left(\frac{1}{n}RSS\right) \tag{7}$$

$$\pi_{AIC} = \frac{L_k}{\sum_{i=1}^{k} L_k} \tag{8}$$

$$L_k = \exp\left(\frac{AIC_{\min} - AIC_k}{2}\right) \tag{9}$$

3 Results and Discussion

The proximate and ultimate analyses of sugarcane bagasse are given in Table 1. The volatile matter and fixed carbon contents were 73.5 and 16.9 wt% on a dry basis (db), respectively, with both carbon and oxygen contents of ~41 wt% (db) as reported elsewhere.[1] The ash content of 9.6 wt% (db) was higher than values previously reported in the literature for sugarcane bagasse (2.0-7.4 wt%),[1,31] but this value has been shown to be dependent on the technique used for the extraction of juice.[1] The sugarcane bagasse ash content was also higher than that of other biomass sources such as switchgrass (6.3 wt%),[25] wheat straw (1.8-3.6 wt%), and corn stover

(2.0 wt%).[32] Sugarcane bagasse had low nitrogen (0.6 wt%, db) and sulfur (0.2 wt%, db) contents, which is beneficial for thermochemical processes in which these species are converted to pollutants including SO_x, NO_x, etc.[33] The ash mainly contained Si, Al, K, Ca, and Mg. Low levels of Fe (< 1.0 mol%) and Ti (< 0.1 mol%) were also detected; rather than being part of the sugarcane structure, however, Fe and Ti originated from the soil and the biomass grinder,[22] respectively.

Although the char devolatilization extent depends on temperature and time, devolatilization is generally complete by 600 °C.[27] The recirculated char in a gasifier will be exposed to temperatures of 750-900 °C and so the sugarcane bagasse char was produced at these temperatures. All char samples had overall mass losses of ~75 wt% and final ash contents of ~35 wt% (db). The elemental compositions of the sugarcane bagasse and char samples were estimated using SEM-EDX and the results are shown in Table 2. For SEM-EDX analysis, the beam penetration depth is only a few nanometers and detection of light elements is limited (due to matrix and absorption effects). Therefore, the EDX elemental determinations of C and O (Table 2) are only estimates for the sample surface and not expected to the be the same as the bulk analysis obtained via ultimate analysis (Table 1).

Table 1. Proximate and ultimate analysis of sugarcane bagasse.

Proximate analysis (wt%)	
Moisture content	6.5 ± 0.1
Volatile matter (db[a])	73.5 ± 1.4
Fixed carbon (db)	16.9 ± 0.9
Ash (db)	9.6 ± 0.8
Ultimate analysis (wt%, db)	

C	41.3 ± 0.3
H	6.4 ± 0.1
O[b]	41.9 ± 0.3
N	0.6 ± 0.0
S	0.2 ± 0.1
Ash	9.6 ± 0.8

225 [a]*db – dry basis.* [b]*Oxygen content was calculated by difference.*

226 **Table 2.** Estimated surface composition of sugarcane bagasse (SCB) and char (as prepared at 750
227 and 850 °C, and after ball milling) as determined by EDX analysis.

Element (mol%)	**SCB**	**char750**	**char850**	**BM-char750**	**BM-char850**
C	53.0 ± 2.0	86.5 ± 1.9	86.9 ± 2.5	64.8 ± 1.0	65.1 ± 1.7
O	46.2 ± 2.1	10.9 ± 1.5	10.8 ± 1.4	26.6 ± 1.8	27.0 ± 2.6
Si	0.4 ± 0.3	1.4 ± 0.8	0.7 ± 0.4	6.1 ± 0.6	5.1 ± 1.0
Al	0.2 ± 0.1	0.7 ± 0.2	0.6 ± 0.3	1.2 ± 0.1	1.0 ± 0.2
K	0.1 ± 0.0	0.2 ± 0.0	0.4 ± 0.3	0.3 ± 0.1	0.2 ± 0.0
Ca	0.02 ± 0.02	0.1 ± 0.0	0.2 ± 0.2	n.d.*	n.d.
Mg	n.d.	0.1 ± 0.1	0.2 ± 0.1	0.1 ± 0.0	0.1 ± 0.0
K/Al	0.4 ± 0.1	0.3 ± 0.1	0.7 ± 0.4	0.2 ± 0.1	0.2 ± 0.0
K/C	0.001	0.002	0.004	0.004	0.002

228 [*]*n.d.: not detected. Individual measurements and elemental composition in wt% provided in*
229 *Supporting Information A.*

230 No significant differences in surface composition were observed between samples produced at
231 different pyrolysis temperatures. The lower oxygen and higher carbon contents of the char in
232 comparison to the sugarcane bagasse (SCB) are a result of the loss of volatile matter. After ball
233 milling, the compositions of the char samples changed again (Table 2). Both the oxygen and
234 silicon contents increased significantly, from 11 to 27 mol% and ~1 to 5-6 mol%, respectively,
235 while the aluminum content increased slightly (~0.7 to 1.1 mol%). Higher Si contents (i.e.,
236 increased Si-O-Si signals) were also observed in the FTIR spectra (Figure 1) after ball milling.[34]

The peaks for aromatic C=C/C=O and phenolic O-H also increased after ball milling, in agreement with previous studies.[19,21] Note, no functional groups were observed in the region of 1800-4000 cm^{-1} in the FTIR spectra.

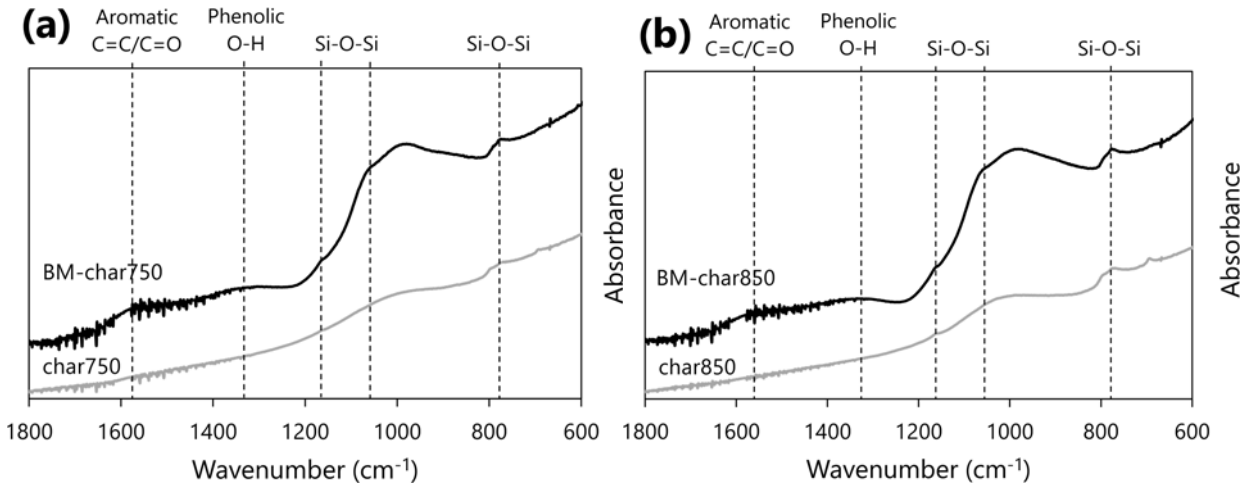

Figure 1. FTIR spectra of sugarcane bagasse char produced at (a) 750 °C and (b) 850 °C, as prepared and ball milled.

Sugarcane bagasse had a heterogeneous morphology (Figure 2a) with two main particle groups: the fibers, which were long (hundreds of microns) particles composed of lignified cell wall layers, and the pith, which were smaller, less dense spherical particles.[1,35] The pyrolysis process did not change the biomass morphology (Figure 2b, fiber and pith remained), as has also been observed for poplar char,[36] but reduced the average particle size from 793 μm to 100 μm. The image in Figure 2b is of a char sample prepared at 750 °C but all the char samples had similar morphologies and size distributions regardless of pyrolysis temperature (i.e., 750-900 °C). Ball milling reduced the char particle size further to less than 10 μm (Figure 2c, which is representative of all the ball-milled char samples), and the fiber and pith were indistinguishable.

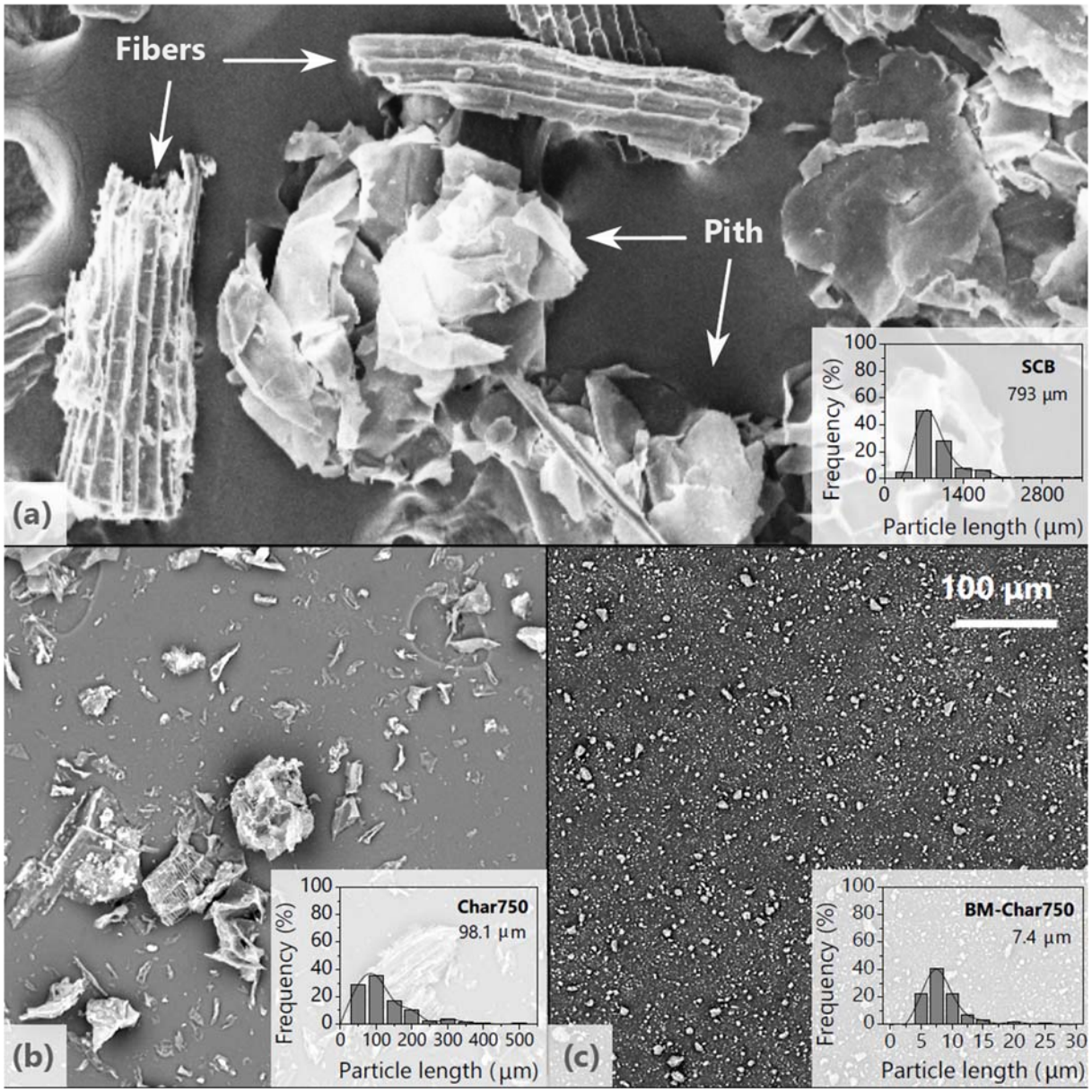

Figure 2. SEM images and particle size distributions of (a) sugarcane bagasse, (b) sugarcane bagasse char as prepared at 750 °C and (c) sugarcane bagasse char prepared at 750 °C and ball milled. The scale bar applies to all images.

Figure 3 is the EDX mapping of sugarcane bagasse char particles (note the difference in the scale bars, which reflects the different particle sizes) prepared at 750 °C before and after ball milling. Whereas C and K are uniformly distributed on all samples, the O, Al, Si are initially in isolated areas and then well-dispersed and much more prominent after ball milling (note the images are representative of five particles per sample mapped and all char samples). A previous

study that used ball milled sugarcane bagasse char as a substitute for carbon black in polymeric composite applications observed dispersed Si agglomerates in micro X-ray tomography and SEM analyses, which were assumed to come from the bagasse char.[22] The ash species are harder than the carbon substrate (for instance, char samples have hardness values of 0.1-5.0 GPa,[37–40] while SiO_2, one of the main species of the char samples in the current study, has hardness values of ~11 GPa).[41]

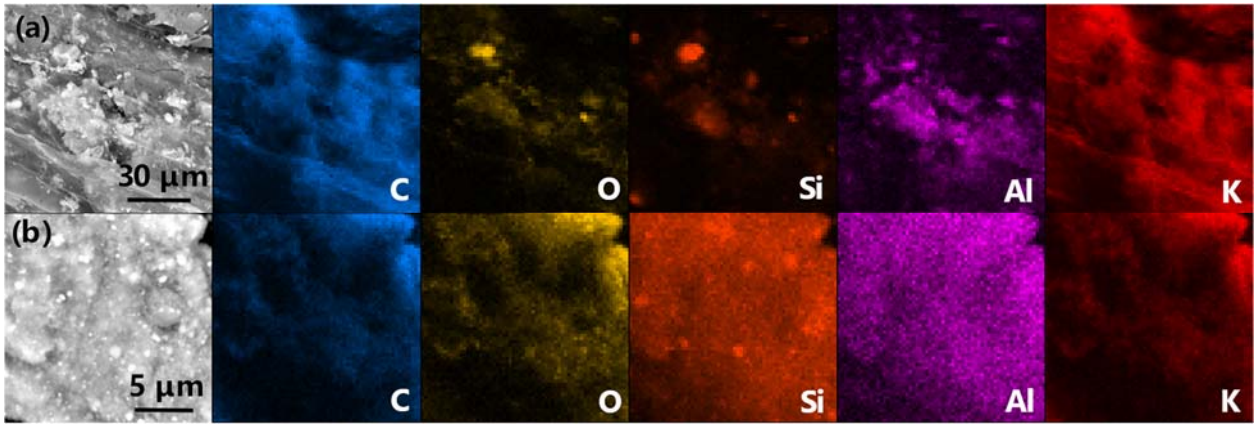

Figure 3. EDX mapping of (a) sugarcane bagasse char as prepared at 750 °C and (b) after ball milling.

The surface areas, pore volumes, and pore size distributions of the char samples were determined using N_2 and CO_2 adsorption data and the results are given in Table 3 and Figure 4. The BET model is generally not suitable for microporous materials,[42] but the values are included for comparison to the literature. The surface areas measured by N_2 adsorption (and fit by the 2D-NLDFT model) decreased from 294 m^2/g to 79 m^2/g as the pyrolysis temperature increased from 750 °C to 900 °C, indicating higher pyrolysis temperatures lead to the partial collapse of the char structure. This result is consistent with the maximum surface areas being achieved at pyrolysis temperatures at or below 700 °C for other biochar materials.[14–17] For example, a study of the effect of pyrolysis temperature on the physical characteristics of safflower seed press cake – a cake obtained from the cold-press extraction of safflower seeds which therefore has a different

structure than sugarcane bagasse – indicated that the BET surface area decreased above a pyrolysis temperature of 700 °C.[43] Pyrolysis temperatures lower than 750 °C were not used because recirculated particles in a fluidized bed gasifier will have experienced temperatures of at least 750 °C. There was not a trend in the surface areas measured by CO_2, which probes the ultramicropores (< 0.7 nm), with the surface areas varying between 403 m^2/g (char900) to 482 m^2/g (char850). Pyrolysis reduces the microporosity of char but has a negligible effect on ultramicroporosity. The micropore volumes and average pore widths determined with 2D-NLDFT calculations using CO_2 adsorption data were similar for all samples (~0.13 cm^3/g and 0.46 nm, respectively).

Table 3. N_2 and CO_2 adsorption results of the sugarcane bagasse char as prepared and after ball milling.

Sample	Surface area (m^2/g)			Micropore volume (cm^3/g)	Pore width (nm)
	2D-NLDFT N_2	BET N_2	2D-NDLFT CO_2	DR CO_2	2D-NDLFT CO_2
char750	294	210	446	0.14	0.47
char800	257	182	406	0.12	0.47
char850	216	372	482	0.13	0.46
char900	79	62	403	0.12	0.46
BM-char750	94	89	189	0.05	0.42
BM-char800	104	96	230	0.05	0.46
BM-char850	172	137	235	0.06	0.46
BM-char900	71	68	123	0.03	0.44

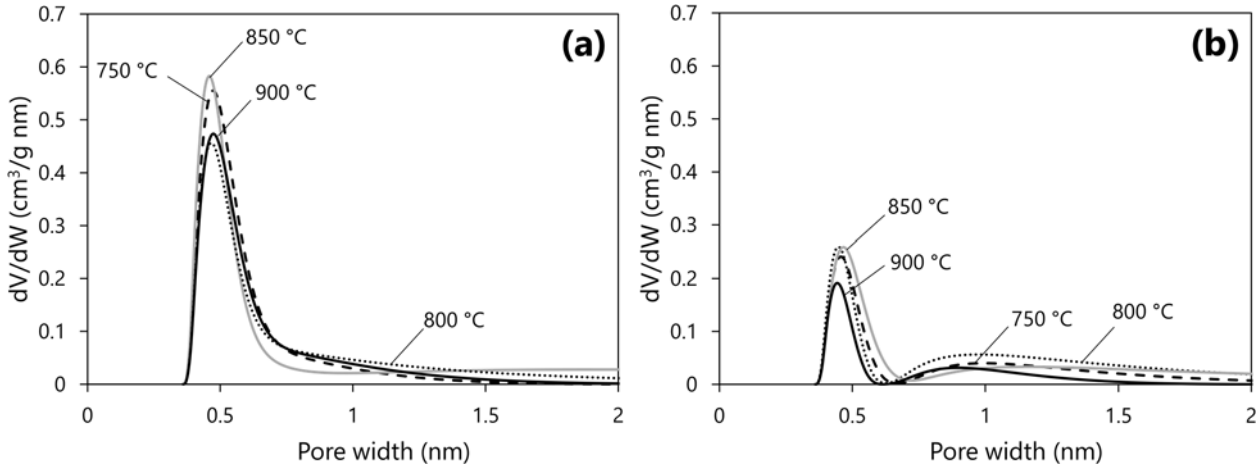

Figure 4. Pore size distributions determined via 2D-NLDFT calculations with CO_2 adsorption data of char samples (a) as prepared and (b) after ball milling.

After ball milling, there was a significant decrease in the number of ultramicropores (i.e., CO_2 uptake) as evidenced by the lower micropore volumes in Table 3 and the normalized adsorption curves using the Dubinin-Radushkevich equation in Supporting Information B. Also, ball milling significantly reduced the surface areas determined by N_2 adsorption (and fit by the 2D-NLDFT model) for the char samples prepared at 750 °C and 800 °C (294 to 94 m^2/g and 257 to 104 m^2/g, respectively); there were smaller decreases in surface area for the samples prepared at 850 °C (216 to 172 m^2/g) and 900 °C (79 to 71 m^2/g). In contrast to pyrolysis, ball milling reduced micro- and ultramicroporosity, possibly due to the accumulation of Si/SiO_2 at the surface of the particles blocking pores. The pore size distributions (Figure 4) reflect these changes after ball milling. In other ball milling studies with sugarcane bagasse char, the samples were prepared at 600 °C,[19,21] and their surface areas did not significantly change after ball milling (359 and 364 m^2/g for unmilled and milled char, respectively, as determined by N_2 adsorption). As mentioned, the physical properties depend on the pyrolysis temperature and so these studies cannot be directly compared to the results obtained herein. Of note, the pore size distributions determined from the N_2 adsorption data as fit with the 2D-NLDFT model are given in Figure B.2

312 (Supporting Information B). As there were only one or two data points for pore widths above 2
313 nm, the pore size distributions with N_2 adsorption data are likely inaccurate for most of the
314 samples.

315 Isothermal gasification of the char samples was carried out at 850 °C with CO_2, and carbon
316 conversion rates as a function of conversion are shown in Figure 5 for the char samples. For the
317 as-prepared samples (Figure 5a), the rates of gasification decreased with pyrolysis temperature
318 up to ~20 % conversion and were proportional to the surface areas determined by N_2 adsorption
319 (Table 3). In the non-isothermal CO_2 gasification of sugarcane bagasse char, Edreis *et al.*
320 suggested that increasing pyrolysis temperatures increased the thermal stability of the carbon
321 structure with a subsequent reduction in the reactivity of the char.[9] The rates were similar to
322 those observed for switchgrass char gasified with CO_2 (maximum of 0.03 min^{-1}),[26] as well as
323 other char gasified with steam including bamboo (maximum of 0.04 min^{-1}), sugarcane bagasse
324 and rice husk (maximum of ~0.02 min^{-1}), and corncob and Hinoki cypress sawdust (maximum of
325 0.015 min^{-1}).[44] The rates for the char samples prepared at temperatures up to 850 °C
326 monotonically decreased with conversion, with the exception of the char sample prepared at 900
327 °C, which went through a maximum at ~10% conversion. This type of gasification behavior has
328 been previously observed for char materials that, like sugarcane bagasse, have Si as the most
329 abundant ash species.[44,45] As shown in Figure 5a, above 30% conversion, the gasification rates
330 were similar and complete gasification required approximately 140 min for all samples. A time
331 of 50 min was reported for the non-isothermal (heating rate of 20 °C min^{-1}) CO_2 gasification of
332 sugarcane bagasse char prepared at 500, 800, and 900 °C but with smaller initial particle sizes in
333 the range of 180-450 μm (compared to the average particle size of 793 μm used herein, Figure
334 2a) and higher gasification temperatures (up to 1300 °C compared to 850 °C used herein).[9]

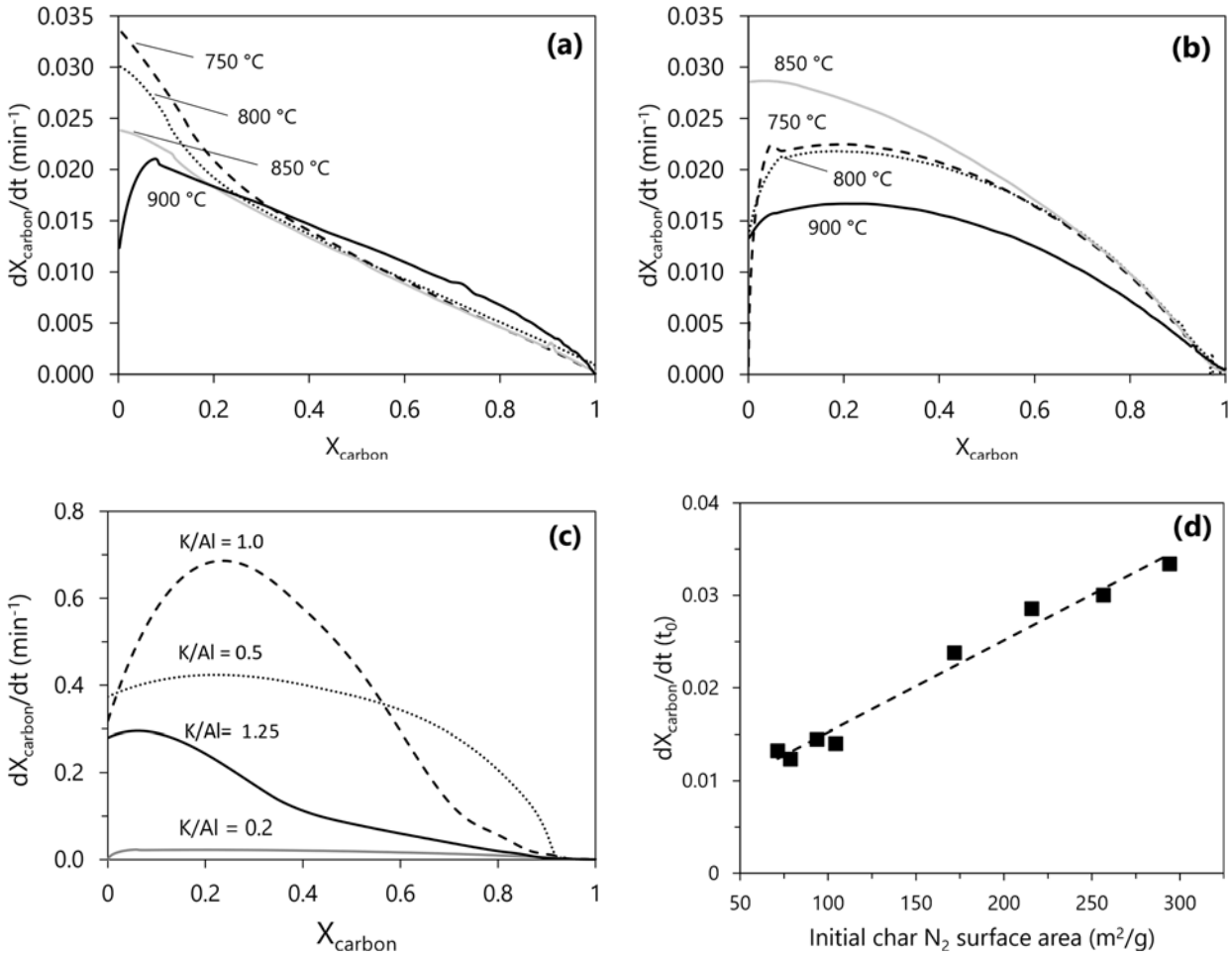

Figure 5. CO_2 gasification rates at 850 °C as a function of carbon conversion for sugarcane bagasse char (a) as prepared, (b) after ball milling, and (c) after ball milling with different KOH loadings; and (d) initial carbon conversion rates as a function of initial char surface area (before gasification) for char samples as prepared and ball milled without KOH. In (a) and (b), the labels on the curves refer to the pyrolysis temperatures used to prepare the samples. In (c), the char samples were prepared at 750 °C and then ball milled with various amounts of KOH (the curve for K/Al = 0.2 corresponds to the char with no additional K, BM-char750). In (d), the surface areas were determined using N_2 adsorption (2D-NLDFT N_2 values in Table 3).

After ball milling, the gasification curves were concave down-shaped with maximum rates at ~20% conversion, except for the char produced at 850 °C, for which the initial rate was the maximum rate (Figure 5b). This sample had the highest surface area (172 m^2/g, Table 3). There was a positive correlation between the initial surface area (as measured by N_2) and the initial gasification rate for all samples (Figure 5d), consistent with gasification under a kinetically controlled regime. Therefore, for the samples without KOH, the gasification curves can be

interpreted as an indirect measure of porosity and surface area changes. For the char samples as prepared at 750, 800 or 850 °C, the highest reaction rate occurs at $t = 0$, indicating that the highest porosity existed at the beginning of the process. The gasification curves of the ball milled samples, however, have concave shapes, which suggests that porosity developed during gasification up to ~20% conversion.

Ball milling reduced the particle sizes (Figure 2c) and porosities (Table 3), while resulting in more oxygen functional groups at the surface (Figure 1 and Table 2). The mass losses during heating to the gasification temperature were higher for the ball milled samples (11-15 wt% versus 2.6-5.7 wt% for the unmilled samples) consistent with the increased oxygen groups. These groups likely devolatilized and or/reacted with the carbon during heating and had a minimal effect on the calculated gasification rates.

Table 4. Initial K/Al ratios estimated by EDX, and time required for 50% ($t_{0.5}$) and 90% ($t_{0.9}$) carbon conversion for sugarcane bagasse char samples gasified with CO_2 at 850 °C.

Sample	KOH loading (wt%)	K/Al		K/C		$t_{0.5}$ (min)	$t_{0.9}$ (min)
		Target	EDX	Target	EDX		
BM-char750 with[a]							
K/Al = 0.2*	0	0.2	0.2	0.004	0.004	24	60
K/Al = 0.5	19	0.5	2.4	0.009	0.028	1.2	3
K/Al = 1.0	53	1.0	15	0.018	0.13	0.9	7
K/Al = 1.25	70	1.25	43	0.023	0.41	3.0	21

[a]K/Al of 0.2, 0.5, 1.0, and 1.25 correspond to KOH loadings of 0, 19, 35, and 70 wt%, respectively.
**same sample as BM-char750.*

Ball milling had the greatest negative impact on the initial gasification rates of char produced at 750 °C (Figure 5a) and so this char was used to test the efficacy of catalyst addition. Char750 was ball milled with different amounts of KOH and the gasification rates of these mixtures as a function of conversion are shown in Figure 5c, while the particle sizes and times required to

reach 50% and 90% conversion are shown in Table 4. The char samples containing K/Al ratios of 0.5, 1.0, and 1.25 had 19, 30, and 13-fold, respectively, increases in maximum rates compared to the original ball milled char (K/Al ratio of 0.2, Table 2). These maximum rates occurred before 50% conversion, in agreement with previous gasification studies with potassium-catalyzed ash-free carbon black,[46] Genesse raw coal,[47] and switchgrass char.[25,26] The char with a K/Al ratio of 0.5 had a maximum rate at ~20% conversion but the rate was relatively constant between 0 and ~50% conversion. In contrast, the samples with K/Al ratios of 1.0 and 1.25 had more distinct maxima at 30% and 10% conversion, respectively and, after gasification, the remaining solids (ash including the added K) were stuck to the cooled crucible. For the other samples, the remaining solids were loose in the bottom of the crucible. Other studies with coal have shown that excess K will sinter and block access of the CO_2.[47] Inhibition effects with high catalyst concentrations have also been reported for the gasification of petcoke and sugarcane bagasse with $FeCl_3$ (> 7 wt% loading).[11] The pure component melting temperature of KOH is 406 °C[48] but K may exist in other forms, including K_2CO_3, leading to complex phase behavior. Another study reported gasification inhibition due to the formation of K silicates.[49]

As shown in Table 4, potassium was located on the particle surfaces after ball milling – the K/Al and K/C ratios calculated using EDX were an order of magnitude higher than the target loadings. The sample with a K/Al ratio of 1.0 reached 50% conversion the fastest (0.9 min), but the sample with the K/Al ratio of 0.5 was the fastest to reach 90% conversion – 3 min compared to 7 and 21 min for the higher ratios and 60 min with no additional K (Table 4). At the highest two K loadings, the surface K/C ratios were above 0.1, which is the saturation value for K as a catalyst in char gasification as highlighted in a previous study.[24] Thus, K increased the rate but at too high a loading, K hindered the gasification.

The RPM and eRPM (eqs. (5) and (6)) were fit to the gasification data and these fits were evaluated using model discrimination techniques. The model parameters are shown in Table 5 and representative graphical fits with residuals are shown in Figure 6 (all fits given in Supporting Information C). The models capture the gasification behavior with one value for the rate constant (k_j) modulated by mainly the carbon conversion level (X_{carbon}) but also the structural factor (ψ), and two constants (c, p) for the eRPM. The values of k_j followed the same trends as the initial surface areas as illustrated in Figure 5d (i.e., higher surface area correlated with a higher rate). The fits for the ball milled samples, except the sample prepared at 850 °C, had lower k_j values but higher ψ values, which captured the maxima in the curves. A second char sample was produced at 850 °C, the tests and characterizations repeated, and all results confirmed the outlying behavior. Further investigation, beyond the scope of this paper, is required to determine why ball milling had a different effect on this sample.

Table 5. Rate constants (k_j), structural factors (ψ), and empirical parameters (c and p) of the sugarcane bagasse char samples with and without added K, calculated via the random pore (RPM) and extended random pore models (eRPM).

Sample	RPM			eRPM			
	R^2	k_j (min^{-1})[a]	ψ	R^2	ψ	c	p
char750	0.972	$2.6\cdot10^{-2} \pm 1.1\cdot10^{-4}$	0 ± 0	0.994	0 ± 0	0.45 ± 0.01	8.9 ± 0.3
char800	0.974	$2.5\cdot10^{-2} \pm 8.7\cdot10^{-5}$	0 ± 0	0.986	0 ± 0	0.32 ± 0.05	12.9 ± 0.9
char850	0.996	$2.3\cdot10^{-2} \pm 3.4\cdot10^{-5}$	0 ± 0	0.998	0.07 ± 0.00	0.13 ± 0.05	5.6 ± 0.3
char900	0.991	$2.0\cdot10^{-2} \pm 8.6\cdot10^{-5}$	1.21 ± 0.03	0.996	1.22 ± 0.01	-0.46 ± 0.02	69.9 ± 4.2
BM-char750*	0.962	$1.9\cdot10^{-2} \pm 2.4\cdot10^{-4}$	4.07 ± 0.16	0.985	3.92 ± 0.04	-0.92 ± 0.03	120.1 ± 8.3
BM-char800	0.990	$2.0\cdot10^{-2} \pm 1.5\cdot10^{-5}$	3.49 ± 0.07	0.993	3.36 ± 0.02	-0.35 ± 0.02	48.6 ± 4.9
BM-char850	0.996	$3.0\cdot10^{-2} \pm 7.5\cdot10^{-5}$	0.73 ± 0.01	0.997	0.71 ± 0.01	-0.05 ± 0.01	12.0 ± 3.2
BM-char900	0.991	$1.5\cdot10^{-2} \pm 4.6\cdot10^{-5}$	3.40 ± 0.04	0.993	3.42 ± 0.01	-0.15 ± 0.01	47.2 ± 4.7
BM-char750 with[b]							

K/Al = 0.2*	0.962	$1.9 \cdot 10^{-2} \pm 2.4 \cdot 10^{-4}$	4.07 ± 0.16	0.985	3.92 ± 0.04	-0.92 ± 0.03	120.1 ± 8.3
K/Al = 0.5	0.969	$3.8 \cdot 10^{-1} \pm 2.3 \cdot 10^{-3}$	4.02 ± 0.08	0.969	4.02 ± 0.03	-0.03 ± 0.02	21.5 ± 18.7
K/Al = 1.0	0.783	$6.8 \cdot 10^{-1} \pm 9.7 \cdot 10^{-3}$	0.51 ± 0.08	0.852	0.57 ± 0.04	-0.64 ± 0.04	19.9 ± 2.0
K/Al = 1.25	0.862	$2.6 \cdot 10^{-1} \pm 2.1 \cdot 10^{-3}$	0 ± 0	0.909	0 ± 0	0.33 ± 0.02	5.0 ± 0.6

*[a]k_j was fixed in the eRPM calculations. [b]K/Al of 0.2, 0.5, 1.0, and 1.25 correspond to KOH loadings of 0, 19, 35, and 70 wt%, respectively. *Same samples.*

Although the correlation coefficients, R^2, were over 0.95 for all but the samples with the two highest amounts of added K, the RPM did not well represent the initial (to ~20% conversion) gasification behavior of most of the char samples. Using the extended model with the rate constants, k_j, obtained from the RPM, the behavior was more fully represented as depicted in Figure 6 and further shown in Supporting Information C by the lower Akaike information criterion (*AIC*) and relative likelihood (L_k) values, higher Akaike probability share (π_{AIC}),[25,30,47] and more randomly distributed residuals. The determined rate constants for the samples with added K were an order of magnitude higher than those of the other samples. The fit for the sample with a K/Al ratio of 0.5 was very good until a conversion of ~95%, while the fits were very poor for the highest two levels of K (Table 5 and Supporting Information C). The ψ values were similar for K/Al ratios of 0.2 and 0.5 (ψ = ~4) but significantly smaller for the samples with higher levels of K (ψ = 0.5 or 0, respectively), consistent with the excess K increasing mass transfer limitations by blocking access of the gasification agent to carbon, and preventing pore formation. The residuals in Figure 6 showed the most deviation from 0 when below 10% and above 80% conversion. The initial behavior is likely not well-represented by the models due to the displacement of N_2 by CO_2 as the reaction gas is introduced, and a variable CO_2 concentration violates a key assumption of the models. The behavior above 80% conversion is likely due to ash sintering at the surface, since the deviation at high conversion is negligible for

char750, more significant (~0.2%) for BM-char750, and much more significant (up to 10%) for BM-char750 with K/Al = 0.5. That is, the deviation from the model increased with increasing ash content.

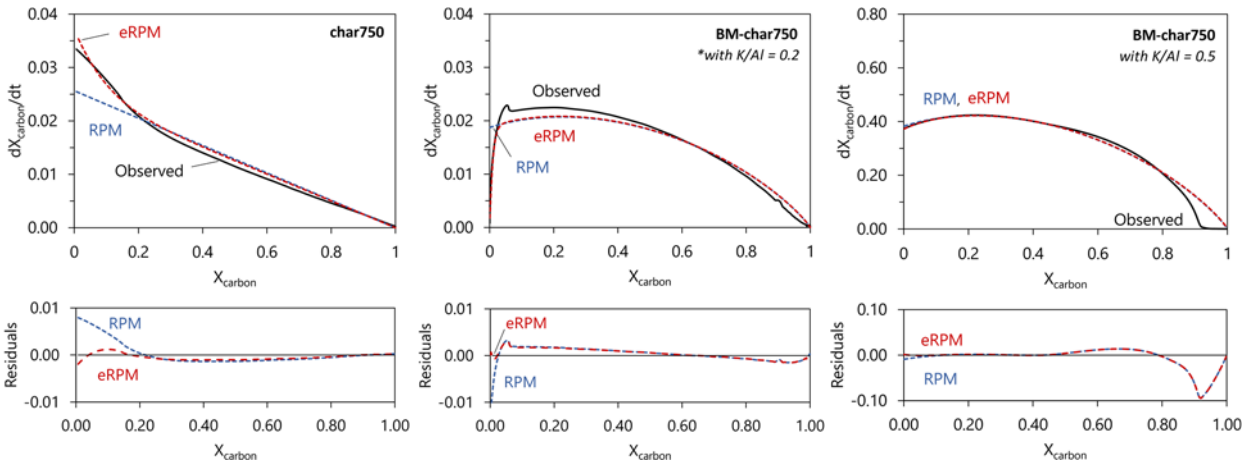

Figure 6. Modeling of the gasification data of char prepared at 750 °C by the RPM and eRPM: fits and residuals. **Same as BM-char750. K/Al = 0.5 (19 wt% KOH loading).*

Particle size and catalyst addition influence the limiting step in gas-solid processes such as gasification, which may be controlled by mass transfer limitations (diffusion of mass and heat through the boundary layer around the char particle or through the porous structure) or the gas-solid reactions with the solid surfaces.[50] The extent of transport limitations is usually tested either by further increasing the flow rate of the gasification agent (CO_2) or the feedstock mass in the TGA unit. Both options were not feasible in this study because the system was already operating at the maximum gas flow rate and increasing the mass of some of the char samples would surpass the maximum feed height in the TGA crucible. Qualitatively, based on the rates and modeling results, gasification of the char samples was likely in a kinetically controlled regime,[51] because the samples had initial particle sizes below 150 μm,[52] the reaction rates were in the order of 10^{-2} min^{-1}, and there was a positive correlation between the initial surface area and initial gasification rates (Figure 5d). In studies with larger particles – biomass wastes of 0.5-8

449 mm diameter[53] and wood char from pressed-oil stone of 0.06-2.1 mm[52] diameter – reactivity
450 decreased with particle size because of mass diffusion. When KOH was added to the char
451 samples, the rate increased likely resulting in a mixed kinetic-transport control regime. The
452 sintering of excess K with higher K/Al ratios and/or high levels of conversion further increased
453 the mass transfer limitations, as highlighted by the decreasing ψ values.
454
455 **4 Conclusions**
456 Sugarcane bagasse char was prepared, characterized, and then gasified in CO_2 at 850 °C to
457 relate the properties of the char to the gasification reactivity. Pyrolysis between 750 and 900 °C
458 resulted in char materials that had similar morphologies and surface compositions. The
459 porosities, however, were different with the surface area/pore volume decreasing as the pyrolysis
460 temperature increased. Ball milling significantly reduced the particle size by almost two orders
461 of magnitude and resulted in increased oxygen and ash (silicon and aluminum) surface
462 concentrations. The surface areas determined by N_2 adsorption significantly decreased for the
463 char samples prepared at 750 or 800 °C, and slightly decreased for the samples prepared at 850
464 and 900 °C. The gasification rates were positively and linearly correlated with the surface areas
465 and the behavior was well modeled by the eRPM. The addition of potassium increased the rates
466 by over an order of magnitude with an optimum level of K/Al ratio between 0.5 and 1 (KOH
467 loadings of 19 and 53 wt%). The gasification behavior was not fully captured by the models at
468 higher potassium loadings likely due to diffusion limitations as the excess K hindered the access
469 of CO_2 to the carbon. These results provide information, regarding char structure, porosity, and
470 reactivity, for the recirculation of char in a gasifier under similar operating conditions as those
471 used in this study. Namely, char produced at higher temperatures will have lower porosity and be
472 less reactive, suggesting optimal operating temperatures $\leq$ 850 °C. Other considerations, such as

heating rates, gas composition, and effects of other oxidizing agents (O_2 and steam), however, should also be included in the design of the gasifier. Particle collisions during recirculation may resemble the effects of ball milling, which resulted in size reduction and increased ash and oxygen surface concentrations. Potassium addition increases the initial gasification rates, but K/Al ratios above 0.5-1 hinder gasification at higher conversions.

ASSOCIATED CONTENT

The following file is available.

Supporting Information (PDF), containing:

Supporting Information A. EDX data of sugarcane bagasse and char samples

Supporting Information B. N_2 and CO_2 adsorption characterization of the char samples

Supporting Information C. Gasification modeling with RPM and eRPM

AUTHOR INFORMATION

Corresponding Author

*Phone: 403-210-9488. Fax: 403-284-4852. E-mail: jhill@ucalgary.ca

Present Addresses

†Laboratory of Optimization, Design, and Advanced Control, School of Chemical Engineering, University of Campinas, Av. Albert Einstein 500, Campinas, 13083-852, Brazil

††Department of Civil & Environmental Engineering, Samueli School of Engineering, University of California, Los Angeles, CA, 90095, USA

Author Contributions

I.L.M. obtained the sugarcane bagasse samples, prepared the char samples, completed the gasification experiments and modeling, performed most of the characterization and prepared the manuscript. R.A.A set up the TGA equipment, developed the gasification method, and revised the manuscript. F.J.L.T. performed the N_2 and CO_2 adsorption experiments, FTIR characterization, and revised the manuscript. R.M.F. and M.R.W.M. provided the equipment for proximate and ultimate analyses and revised the manuscript. J.M.H. obtained all the other equipment for the characterization and tests, provided project funding, supervised the other authors, and revised the manuscript.

Funding Sources

We recognize the funding from CNPq, Coordenação de Aperfeiçoamento de Pessoal de Nível Superior - Brasil (CAPES) - Finance Code 001, São Paulo Research Foundation (FAPESP) grant #2015/20630-4, and Natural Sciences and Engineering Research Council (NSERC) grant RGPIN/05076-2015.

Notes

The authors declare no competing financial interest.

ACKNOWLEDGMENT

The authors would like to thank Dr. Jan Kopyscinski for advice on the kinetic modeling.

REFERENCES

(1) Bizzo, W. A.; Lenço, P. C.; Carvalho, D. J.; Veiga, J. P. S. The Generation of Residual Biomass during the Production of Bio-Ethanol from Sugarcane, Its Characterization and Its Use in Energy Production. *Renew. Sustain. Energy Rev.* **2014**, *29*, 589–603. https://doi.org/10.1016/j.rser.2013.08.056.

(2) Hofsetz, K.; Silva, M. A. Brazilian Sugarcane Bagasse: Energy and Non-Energy Consumption. *Biomass and Bioenergy* **2012**, *46*, 564–573. https://doi.org/10.1016/j.biombioe.2012.06.038.

(3) Klasson, K. T. Char from Sugarcane Bagasse. In *Biorefinery Co-Products: Phytochemicals, Primary Metabolites and Value-Added Biomass Processing*; Bergeron, C., Carrier, D. J., Ramaswamy, S., Eds.; Wiley, 2012; pp 327–350. https://doi.org/10.1002/9780470976692.ch15.

(4) Fan, X.; Yang, L.; Jiang, J. Experimental Study on Industrial-Scale CFB Biomass Gasification. *Renew. Energy* **2020**, *158*, 32–36. https://doi.org/10.1016/j.renene.2020.05.145.

(5) Zhang, C.; Zeng, G.; Huang, D.; Lai, C.; Chen, M.; Cheng, M.; Tang, W.; Tang, L.; Dong, H.; Huang, B.; et al. Biochar for Environmental Management : Mitigating Greenhouse Gas Emissions , Contaminant Treatment , and Potential Negative Impacts. *Chem. Eng. J.* **2019**, *373* (January), 902–922. https://doi.org/10.1016/j.cej.2019.05.139.

(6) Wang, J.; Wang, S. Preparation, Modification and Environmental Application of Biochar: A Review. *J. Clean. Prod.* **2019**, *227*, 1002–1022. https://doi.org/10.1016/j.jclepro.2019.04.282.

(7) Hernández, J. J.; Saffe, A.; Collado, R.; Monedero, E. Recirculation of Char from Biomass Gasification: Effects on Gasifier Performance and End-Char Properties. *Renew. Energy* **2020**, *147*, 806–813. https://doi.org/10.1016/j.renene.2019.09.063.

(8) Edreis, E. M. A.; Luo, G.; Li, A.; Chao, C.; Hu, H.; Zhang, S.; Gui, B.; Xiao, L.; Xu, K.; Zhang, P.; et al. CO2 Co-Gasification of Lower Sulphur Petroleum Coke and Sugar Cane Bagasse via TG– FTIR Analysis Technique. *Bioresour. Technol.* **2013**, *136*, 595–603. https://doi.org/10.1016/j.biortech.2013.02.112.

(9) Edreis, E. M. A.; Luo, G.; Yao, H. Investigations of the Structure and Thermal Kinetic Analysis of Sugarcane Bagasse Char during Non-Isothermal CO2 Gasification. *J. Anal. Appl. Pyrolysis* **2014**, *107*, 107–115. https://doi.org/10.1016/j.jaap.2014.02.010.

(10) Edreis, E. M.; Yao, H. Kinetic Thermal Behaviour and Evaluation of Physical Structure of Sugar Cane Bagasse Char during Non-Isothermal Steam Gasification. *J. Mater. Res. Technol.* **2016**, *5* (4), 317–326. https://doi.org/10.1016/j.jmrt.2016.03.006.

(11) Edreis, E. M. A.; Li, X.; Xu, C.; Yao, H. Kinetic Study and Synergistic Interactions on Catalytic CO2 Gasification of Sudanese Lower Sulphur Petroleum Coke and Sugar Cane Bagasse. *J. Mater. Res. Technol.* **2017**, *6* (2), 147–157. https://doi.org/10.1016/j.jmrt.2016.09.001.

(12) Edreis, E. M. A.; Li, X.; Luo, G.; Sharshir, S. W.; Yao, H. Kinetic Analyses and Synergistic Effects of CO2 Co-Gasification of Low Sulphur Petroleum Coke and Biomass Wastes. *Bioresour. Technol.* **2018**, *267*, 54–62. https://doi.org/10.1016/j.biortech.2018.06.089.

(13) Bhatia, S. K.; Perlmutter, D. D. A Random Pore Model for Fluid-Solid Reactions: I.

Isothermal, Kinetic Control. *AIChE J.* **1980**, *26* (3), 379–386. https://doi.org/10.1007/978-3-319-89554-3.

(14) Mukherjee, A.; Zimmerman, A. R.; Harris, W. Surface Chemistry Variations among a Series of Laboratory-Produced Biochars. *Geoderma* **2011**, *163* (3–4), 247–255. https://doi.org/10.1016/j.geoderma.2011.04.021.

(15) Ahmad, M.; Soo, S.; Dou, X.; Mohan, D.; Sung, J.; Yang, J. E.; Ok, Y. S. Effects of Pyrolysis Temperature on Soybean Stover- and Peanut Shell-Derived Biochar Properties and TCE Adsorption in Water. *Bioresour. Technol.* **2012**, *118*, 536–544. https://doi.org/10.1016/j.biortech.2012.05.042.

(16) Zhao, L.; Cao, X.; Masek, O.; Zimmerman, A. Heterogeneity of Biochar Properties as a Function of Feedstock Sources and Production Temperatures. *J. Hazard. Mater.* **2013**, *257*, 1–9. https://doi.org/10.1016/j.jhazmat.2013.04.015.

(17) Gray, M.; Johnson, M. G.; Dragila, M. I.; Kleber, M. Water Uptake in Biochars: The Roles of Porosity and Hydrophobicity. *Biomass and Bioenergy* **2014**, *61*, 196–205. https://doi.org/10.1016/j.biombioe.2013.12.010.

(18) Xu, X.; Zheng, Y.; Gao, B.; Cao, X. N-Doped Biochar Synthesized by a Facile Ball-Milling Method for Enhanced Sorption of CO2 and Reactive Red. *Chem. Eng. J.* **2019**, *368* (February), 564–572. https://doi.org/10.1016/j.cej.2019.02.165.

(19) Lyu, H.; Gao, B.; He, F.; Zimmerman, A. R.; Ding, C.; Huang, H.; Tang, J. Effects of Ball Milling on the Physicochemical and Sorptive Properties of Biochar: Experimental Observations and Governing Mechanisms. *Environ. Pollut.* **2018**, *233*, 54–63.

https://doi.org/10.1016/j.envpol.2017.10.037.

(20) Lyu, H.; Gao, B.; He, F.; Zimmerman, A. R.; Ding, C.; Tang, J.; Crittenden, J. C. Experimental and Modeling Investigations of Ball-Milled Biochar for the Removal of Aqueous Methylene Blue. *Chem. Eng. J.* **2018**, *335*, 110–119. https://doi.org/10.1016/j.cej.2017.10.130.

(21) Lyu, H.; Yu, Z.; Gao, B.; He, F.; Huang, J.; Tang, J.; Shen, B. Ball-Milled Biochar for Alternative Carbon Electrode. *Environ. Sci. Pollut. Res.* **2019**, *26*, 14693–14702. https://doi.org/10.1007/s11356-019-04899-4.

(22) Ferreira, G. F.; Pierozzi, M.; Fingolo, A. C.; da Silva, W. P.; Strauss, M. Tuning Sugarcane Bagasse Biochar into a Potential Carbon Black Substitute for Polyethylene Composites. *J. Polym. Environ.* **2019**, *27* (8), 1735–1745. https://doi.org/10.1007/s10924-019-01468-1.

(23) Arnold, R. A.; Hill, J. M. Catalysts for Gasification: A Review. *Sustain. Energy Fuels* **2019**, *3*, 656–672. https://doi.org/10.1039/c8se00614h.

(24) Karlström, O.; Dirbeba, M. J.; Costa, M.; Brink, A.; Hupa, M. Influence of K/C Ratio on Gasification Rate of Biomass Chars. *Energy & Fuels* **2018**, *32*, 10695−10700. https://doi.org/10.1021/acs.energyfuels.8b02288.

(25) Arnold, R. A.; Habibi, R.; Kopyscinski, J.; Hill, J. M. Interaction of Potassium and Calcium in the Catalytic Gasification of Biosolids and Switchgrass. *Energy & Fuels* **2017**, *31*, 6240–6247. https://doi.org/10.1021/acs.energyfuels.7b00972.

(26) Habibi, R.; Kopyscinski, J.; Masnadi, M. S.; Lam, J.; Grace, J. R.; Mims, C. A.; Hill, J. M. Co-Gasification of Biomass and Non-Biomass Feedstocks: Synergistic and Inhibition

599 Effects of Switchgrass Mixed with Sub-Bituminous Coal and Fluid Coke During CO2
600 Gasification. *Energy & Fuels* **2013**, *27*, 494−500. https://doi.org/10.1021/ef301567h.

601 (27) Venderbosch, R. H.; Prins, W. Fast Pyrolysis. In *Thermochemical Processing of Biomass:*
602 *Conversion into Fuels, Chemicals and Power*; Brown, R. C., Ed.; John Wiley & Sons:
603 Chichester, 2011; pp 124–156. https://doi.org/10.1002/9781119990840.ch5.

604 (28) Edreis, E. M. A.; Luo, G.; Li, A.; Xu, C.; Yao, H. Synergistic Effects and Kinetics Thermal
605 Behaviour of Petroleum Coke/Biomass Blends during H2O Co-Gasification. *Energy*
606 *Convers. Manag.* **2014**, *79*, 355–366. https://doi.org/10.1016/j.enconman.2013.12.043.

607 (29) Bhatia, S. K.; Vartak, B. J. Reaction of Microporous Solids: The Discrete Random Pore
608 Model. *Carbon N. Y.* **1996**, *34* (11), 1383–1391. https://doi.org/10.1016/S0008-
609 6223(96)00080-2.

610 (30) Kopyscinski, J.; Habibi, R.; Mims, C. A.; Hill, J. M. K2CO3 - Catalyzed CO2 Gasification
611 of Ash-Free Coal: Kinetic Study. *Energy & Fuels* **2013**, *27*, 4875−4883.
612 https://doi.org/10.1021/ef400552q.

613 (31) de Medeiros, E. M.; Posada, J. A.; Noorman, H.; Osseweijer, P.; Filho, R. M. Hydrous
614 Bioethanol Production from Sugarcane Bagasse via Energy Self-Sufficient Gasification-
615 Fermentation Hybrid Route: Simulation and Financial Analysis. *J. Clean. Prod.* **2017**, *168*,
616 1625–1635. https://doi.org/10.1016/j.jclepro.2017.01.165.

617 (32) Hernández, C.; Escamilla-Alvarado, C.; Sánchez, A.; Alarcón, E.; Ziarelli, F.; Musule, R.;
618 Valdez-Vazquez, I. Wheat Straw, Corn Stover, Sugarcane, and Agave Biomasses: Chemical
619 Properties, Availability, and Cellulosic-Bioethanol Production Potential in Mexico.

Biofuels, Bioprod. Biorefining **2019**, *13* (5), 1143–1159. https://doi.org/10.1002/bbb.2017.

(33) Asadullah, M. Biomass Gasification Gas Cleaning for Downstream Applications: A Comparative Critical Review. *Renew. Sustain. Energy Rev.* **2014**, *40*, 118–132. https://doi.org/10.1016/j.rser.2014.07.132.

(34) Tahiri, N.; Khouchaf, L.; Elaatmani, M.; Louarn, G.; Zegzouti, A.; Daoud, M. Study of the Thermal Treatment of SiO2 Aggregate. *IOP Conf. Ser. Mater. Sci. Eng.* **2014**, *62* (1). https://doi.org/10.1088/1757-899X/62/1/012002.

(35) Nebra, S. A.; Macedo, I. de C. Bagasse Particles Shape and Size and Their Free-Settling Velocity. *Int. Sugar J.* **1987**, *90* (1077), 168–170.

(36) Wu, R.; Beutler, J.; Price, C.; Baxter, L. L. Biomass Char Particle Surface Area and Porosity Dynamics during Gasification. *Fuel* **2020**, *264* (December 2019), 116833. https://doi.org/10.1016/j.fuel.2019.116833.

(37) Das, O.; Sarmah, A. K.; Bhattacharyya, D. Structure-Mechanics Property Relationship of Waste Derived Biochars. *Sci. Total Environ.* **2015**, *538*, 611–620. https://doi.org/10.1016/j.scitotenv.2015.08.073.

(38) Wallace, C. A.; Saha, G. C.; Afzal, M. T.; Lloyd, A. Experimental and Computational Modeling of Effective Flexural/Tensile Properties of Microwave Pyrolysis Biochar Reinforced GFRP Biocomposites. *Compos. Part B Eng.* **2019**, *175* (April), 107180. https://doi.org/10.1016/j.compositesb.2019.107180.

(39) Wallace, C. A.; Afzal, M. T.; Saha, G. C. Effect of Feedstock and Microwave Pyrolysis Temperature on Physio-Chemical and Nano-Scale Mechanical Properties of Biochar.

Bioresour. Bioprocess. **2019**, *6* (1). https://doi.org/10.1186/s40643-019-0268-2.

(40) Zickler, G. A.; Schöberl, T.; Paris, O. Mechanical Properties of Pyrolysed Wood: A Nanoindentation Study. *Philos. Mag.* **2006**, *86* (10), 1373–1386. https://doi.org/10.1080/14786430500431390.

(41) MEMSnet. Material: Silicon Dioxide (SiO2), bulk https://www.memsnet.org/material/silicondioxidesio2bulk/.

(42) Rouquerol, J.; Llewellyn, P.; Rouquerol, F. *Is the BET Equation Applicable to Microporous Adsorbents?*; Elsevier B.V., 2007; Vol. 160. https://doi.org/10.1016/s0167-2991(07)80008-5.

(43) Angın, D. Effect of Pyrolysis Temperature and Heating Rate on Biochar Obtained from Pyrolysis of Safflower Seed Press Cake. *Bioresour. Technol.* **2013**, *128*, 593–597. https://doi.org/10.1016/j.biortech.2012.10.150.

(44) Zhang, Y.; Ashizawa, M.; Kajitani, S.; Miura, K. Proposal of a Semi-Empirical Kinetic Model to Reconcile with Gasification Reactivity Profiles of Biomass Chars. *Fuel* **2008**, *87* (4–5), 475–481. https://doi.org/10.1016/j.fuel.2007.04.026.

(45) Romero Millán, L. M.; Sierra Vargas, F. E.; Nzihou, A. Catalytic Effect of Inorganic Elements on Steam Gasification Biochar Properties from Agrowastes. *Energy and Fuels* **2019**, *33* (9), 8666–8675. https://doi.org/10.1021/acs.energyfuels.9b01460.

(46) Arnold, R. A.; Hill, J. M. Effect of Calcium and Barium on Potassium-Catalyzed Gasification of Ash-Free Carbon Black. *Fuel* **2019**, *254*, 115647. https://doi.org/10.1016/j.fuel.2019.115647.

(47) Islam, S.; Kopyscinski, J.; Liew, S. C.; Hill, J. M. Impact of K2CO3 Catalyst Loading on the CO2-Gasification of Genesse Raw Coal and Low-Ash Product. *Powder Technol.* **2016**, *290*, 141–147. https://doi.org/10.1016/j.powtec.2015.12.013.

(48) Haynes, W. *CRC Handbook of Chemistry and Physics*, 95th ed.; Haynes, W., Ed.; CRC Press LLC: Boca Raton, 2014.

(49) Strandberg, A.; Holmgren, P.; Wagner, D. R.; Molinder, R.; Wiinikka, H.; Umeki, K.; Broström, M. Effects of Pyrolysis Conditions and Ash Formation on Gasification Rates of Biomass Char. *Energy and Fuels* **2017**, *31* (6), 6507–6514. https://doi.org/10.1021/acs.energyfuels.7b00688.

(50) Laurendeau, N. M. Heterogeneous Kinetics of Coal Char Gasification and Combustion. *Prog. Energy Combust. Sci.* **1978**, *4*, 221–270. https://doi.org/10.1016/0360-1285(78)90008-4.

(51) Adschiri, T.; Furusawa, T. Relation between CO2-Reactivity of Coal Char and BET Surface Area. *Fuel* **1986**, *65* (7), 927–931. https://doi.org/10.1016/0016-2361(86)90200-0.

(52) Gómez-Barea, A.; Ollero, P.; Fernández-Baco, C. Diffusional Effects in CO2 Gasification Experiments with Single Biomass Char Particles. 1. Experimental Investigation. *Energy and Fuels* **2006**, *20* (5), 2202–2210. https://doi.org/10.1021/ef050365a.

(53) Hernández, J. J.; Aranda-Almansa, G.; Bula, A. Gasification of Biomass Wastes in an Entrained Flow Gasifier: Effect of the Particle Size and the Residence Time. *Fuel Process. Technol.* **2010**, *91* (6), 681–692. https://doi.org/10.1016/j.fuproc.2010.01.018.